Hindawi Publishing Corporation
Mathematical Problems in Engineering
Volume 2013, Article ID 369504, 8 pages
http://dx.doi.org/10.1155/2013/369504

Research Article

Design and Analysis of a Novel Speed-Changing Wheel Hub with an Integrated Electric Motor for Electric Bicycles

Yi-Chang Wu and Zi-Heng Sun

Department of Mechanical Engineering, National Yunlin University of Science & Technology, Yunlin 640, Taiwan

Correspondence should be addressed to Yi-Chang Wu; wuyc@yuntech.edu.tw

Received 9 September 2013; Accepted 10 October 2013

Academic Editor: Teen-Hang Meen

The aim of this paper is to present an innovative electromechanical device which integrates a brushless DC (BLDC) hub motor with a speed-changing wheel hub stored on the rear wheel of an electric bicycle. It combines a power source and a speed-changing mechanism to simultaneously provide functions of power generation and transmission for electric bicycles. As part of the proposed integrated device, the wheel hub consists of a basic planetary gear train providing three forward speeds including a low-speed gear, a direct drive, and a high-speed gear. Each gear is manually controlled by the shift control sleeve to selectively engage or disengage four pawl-and-ratchet clutches based on its clutching sequence table. The number of gear teeth of each gear element of the wheel hub is synthesized. The BLDC hub motor is an exterior-rotor-type permanent-magnet synchronous motor. Two-dimensional finite-element analysis (FEA) software is employed to facilitate the motor design and performance analysis. An analysis of the power transmission path at each gear is provided to verify the validity of the proposed design. The results of this work are beneficial to the embodiment, design, and development of novel electromechanical devices for the power and transmission systems of electric bicycles.

1. Introduction

An electric bicycle is a bicycle with an integrated electric motor which can be used for urban transportation, propulsion, and recreation. Except for those with direct-driven hub motors, electric bicycles are typically equipped with speed-changing devices to mechanically adjust the rotational speed of the rear wheel. Since the efficiency of an electric motor is related to its rotational speed, an electric bicycle further provides a mechanical speed-changing device for transmission enabling the electric motor to operate in its most efficient state and, hence, leads to longer periods of use before the battery needs to be charged. As can be seen in the existing products [1], the electric motor and the speed-changing device of an electric bicycle, which are, respectively, used for power generation and transmission, make up individual electrical and mechanical devices. The driving power generated by the electric motor is mostly transmitted from the front chain-wheel at the crankset to the rear sprocket installed on the rear wheel via a chain mechanism. The main drawback of such a conventional design is the lengthy power transmission path from the electric motor to the speed-changing device using a sprocket and chain mechanism, which may cause additional mechanical energy losses due to friction. A second drawback is the cumbersome workspace arrangement due to the individual design of the electric motor and the speed-changing device. Hence, the integration of the electric motor and the speed-changing device for electric bicycles is worth studying. Upon investigating existing electric bicycles, we found that they usually employ the rear derailleur system as the mechanical speed-changing device to provide a set of speed ratios. Unfortunately, the derailleur, the chain, and sprockets are all exposed to the elements. Rain and musk usually stick to the shifter and may damage the derailleur. Therefore, the derailleur mechanism needs to be regularly maintained. In contrast, the speed-changing wheel hub, which is implemented with a planetary gear train and a speed-changing control mechanism, is immune to contamination due to the protection of the hub shell. Such a kind of internal transmission hub for electric bicycles

has the unique advantages of compact size, good reliability, and high efficiency [2–4]. One special feature of the speed-changing wheel hub is that it can change gear ratios when the rear wheel is not rotating. This can be very useful for a commuter with frequent stop-and-go riding in urban areas. Because the speed-changing wheel hub generally has a long maintenance-free life, it is the subject of ongoing research by commercial organizations and academic institutions. As for the power source of electric bicycles, several types of electric motors, including brush DC motors, induction motors, reluctance motors, and brushless permanent-magnet motors, are employed in existing products for traction. Among these electric motors, brushless DC (BLDC) motors have attracted increasing interest due to the characteristics of high efficiency, low cost of maintenance, light weight, easy speed control, and low noise and vibration [5, 6]. Due to these reasons, the BLDC motor and the speed-changing wheel hub are designated as the objects of this study. In addition, the integration of the BLDC motor and the speed-changing wheel hub for electric bicycles may offer new opportunities to overcome the above shortcomings of existing products.

The purpose of this paper is to develop a novel electromechanical device by combining an electric motor with a speed-changing wheel hub for electric bicycles to overcome the drawbacks of traditional designs. An integrated design that combines an exterior-rotor BLDC hub motor within a three-speed wheel hub resulting in a compact power generation and transmission device is introduced. The configuration, operational principles, and qualitative features of the proposed design are addressed. A clutching sequence table is synthesized to provide three forward speeds. The embodiment design of a speed-changing wheel hub, that comprises a basic planetary gear train and a speed-changing control mechanism, is presented. Besides, a 350 W, 3-phase, 12-pole/18-slot BLDC hub motor with an exterior-rotor configuration is designed as part of the integrated device, and the electromagnetic torque of this motor is calculated by finite-element analysis (FEA). Finally, the power transmission path at each speed is illustrated to verify the feasibility of the integrated device.

2. A Novel Design Concept

By integrating a 3-phase, 12-pole/18-slot exterior-rotor BLDC hub motor within a three-speed wheel hub, an electromechanical device with a compact structure is proposed. This integrated device is stored on the rear wheel of the electric bicycle. Figures 1(a), 1(b), and 1(c), respectively, show an exploded view, a cutaway view, and a longitudinal sectional view of the proposed design concept. For the three-speed wheel hub, it consists of a two degrees-of-freedom (DOF) basic planetary gear train, which is the main body of the wheel hub and a speed-changing control mechanism to carry out a power source impartation. The basic planetary gear train is the simplest geared mechanism in the planetary gear train family, which comprises a stationary hub shaft (Member 0) mounted to the rear fork of the electric bicycle, a planet gear (Member 4) engaged with a sun gear (Member 1) and a ring gear (Member 2), and a planet arm (Member 3) to maintain a constant distance between the sun gear (Member 1) and the planet gear (Member 4). The sun gear (Member 1), the ring gear (Member 2), and the planet arm (Member 3) all rotate about the stationary hub shaft (Member 0); they are called coaxial links. Only coaxial links can be used as the input, output, or fixed links of a transmission due to the engineering reality [7, 8]. To obtain a predictable output with this two-DOF planetary gear train, two independent inputs, including one input link and one fixed link, are required. The sun gear (Member 1) is designated as the fixed link since it is mounted to the stationary hub shaft (Member 0). The ring gear (Member 2) or the planet arm (Member 3) serves as the input link or the output link. Once the ring gear (Member 2) is designated as the input link, then the planet arm (Member 3) becomes the output link, and vice versa. The speed-changing control mechanism consists of a shift control sleeve (Member 8) to selectively control the engagement or the disengagement of two one-way clutches, including an input pawl-and-ratchet clutch (Member C_{i3}) and an output pawl-and-ratchet clutch (Member C_{o2}), and a compression spring (Member 13) attached to the right side of the shift control sleeve (Member 8). As illustrated in Figure 2, the right side of the shift control sleeve (Member 8) disposes of a plurality of keys to transfer the rotational power from the rotor yoke (Member 6). In the middle of the shift control sleeve (Member 8), a circular flange is configured to control the engagement or the disengagement of an output pawl-and-ratchet clutch (Member C_{o2}). The left side of the shift control sleeve (Member 8) circularly disposes of pawls which are used to engage with the ratchet arranged in the inner periphery of the planet arm (Member 3) to form an input pawl-and-ratchet clutch (Member C_{i3}). The activation of clutches C_{o2} and C_{i3} is controlled by the axially relative position of the shift control sleeve (Member 8) and the stationary hub shaft (Member 0). The main components of the exterior-rotor BLDC hub motor are a rotor (Member 6) and a stator (Member 5). Twelve permanent magnets (Member 7) are affixed to the inner surface of the rotor yoke (Member 6) to prevent the magnets from flying apart, especially in high-speed applications. In contrast to a traditional interior-rotor BLDC motor, the relatively large rotor diameter increases the moment of inertia, which in turn helps maintain a constant rotational speed. The rotor yoke (Member 6) is engaged with the ring gear (Member 2) by an input pawl-and-ratchet clutch (Member C_{i2}) and is engaged with the shift control sleeve (Member 8) by a plurality of keys on the shift control sleeve (Member 8) and slots on the rotor yoke (Member 6). The stator (Member 5) has eighteen stator slots around which 3-phase winding coils are wound. Both the rotor yoke (Member 6) and the stator (Member 5) are comprised of a lamination of magnetic steel slices to reduce the eddy current losses. In addition, Member 9 is the hub shell of the integrated device, Member 10 is a cover integrated with a bearing seat, Member 11 is the right-side ball bearing, Member 12 is the left-side ball bearing, and Members 14 and 15 are pins for the planet gear (Member 4) and pawls of one-way clutches, respectively. Each speed of the integrated device is governed by the engagement and disengagement of four pawl-and-ratchet clutches C_{i2},

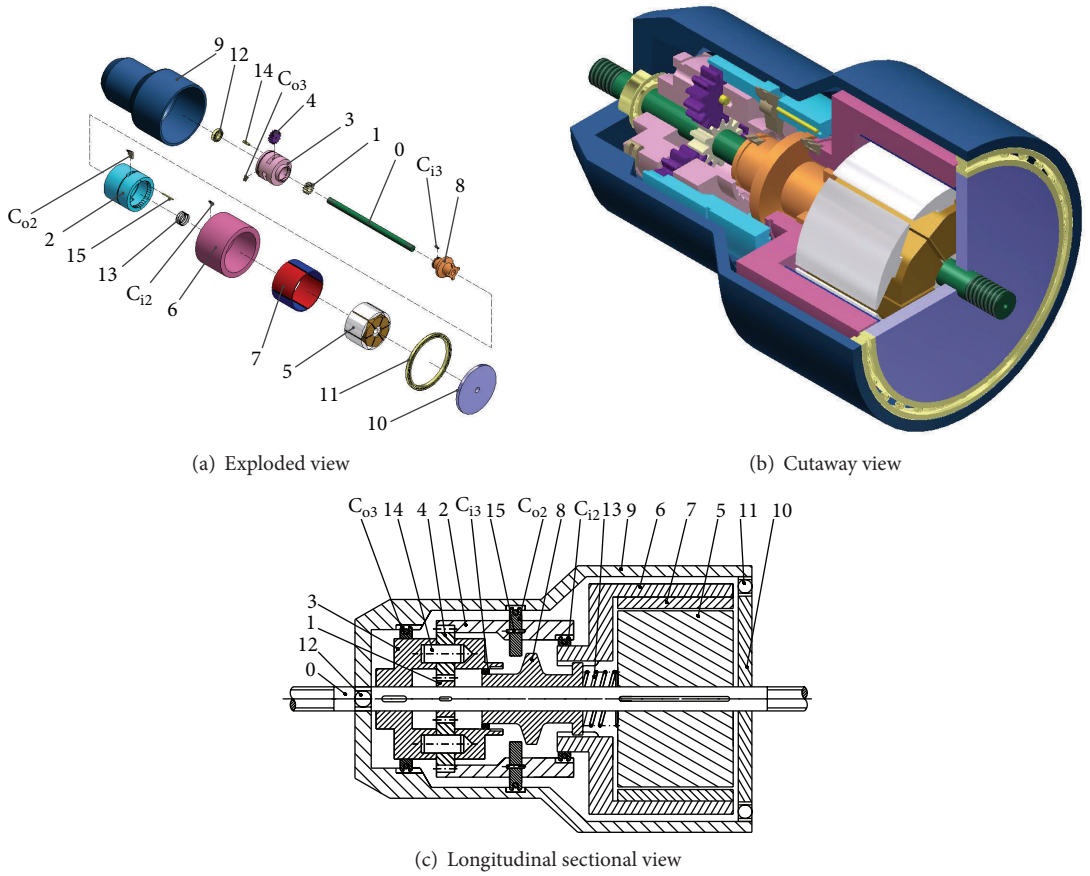

(a) Exploded view

(b) Cutaway view

(c) Longitudinal sectional view

Figure 1: A novel electromechanical device in which a three-speed wheel hub integrates with an exterior-rotor BLDC hub motor.

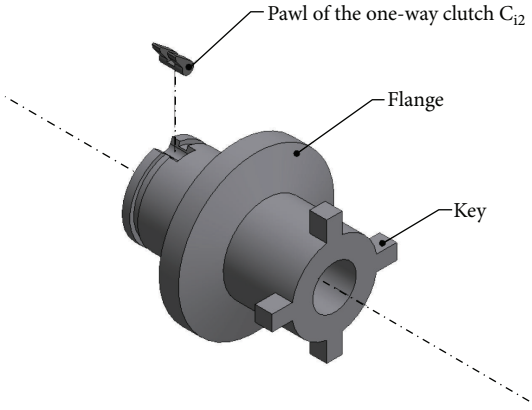

Figure 2: A shift control sleeve (Member 8) of the speed-changing control mechanism of the integrated device.

C_{o2}, C_{i3}, and C_{o3} for proper control of the power transmission path based on the clutching sequence table presented in the following section.

In contrast to individual designs of power generation and transmission systems of existing electric bicycles, the proposed integrated design has the following significant features. (1) The BLDC motor, integrated with a three-speed wheel hub, reduces the use of a chain mechanism and related mechanical fasteners. Fewer mechanical components may decrease production cost, improve the reliability, and make the power and transmission systems more compact and lightweight. (2) The length of the power transfer path from the electric motor to the speed-changing device installed on the rear wheel has shrunk, which also reduces the required space for installation. (3) The proposed design provides three forward speeds. It enables the electric motor to operate in its most efficient state due to the mechanically adjustable speed of the rear wheel by the speed-changing wheel hub.

3. Design of a Three-Speed Wheel Hub

For a 5-link, 2-DOF basic planetary gear train, the related functional schematic is illustrated in Figure 3. The sun gear (Member 1) is adjacent to the planet gear (Member 4) with an external gear pair (Joint a), while the planet gear (Member 4) is adjacent to the ring gear (Member 2) with an internal gear pair (Joint b). A fundamental circuit consists of two meshing gears i and j and one carrier k to maintain a constant center distance between the two gears, which is symbolically denoted as $(i, j)(k)$ [9, 10]. Two fundamental circuits are identified as $(1,4)(3)$ and $(2,4)(3)$, respectively. The corresponding fundamental circuit equations are

$$\begin{aligned} \omega_1 - \gamma_{41}\omega_4 + (\gamma_{41} - 1)\,\omega_3 &= 0, \\ \omega_2 - \gamma_{42}\omega_4 + (\gamma_{42} - 1)\,\omega_3 &= 0, \end{aligned} \tag{1}$$

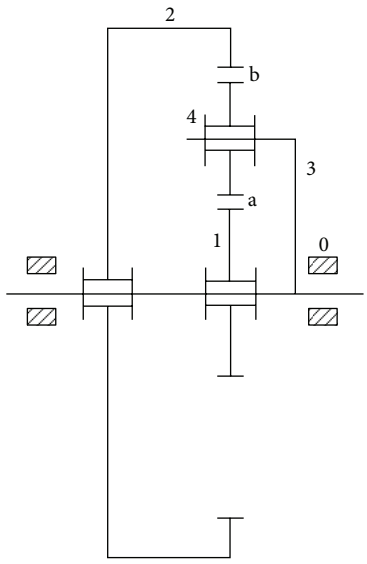

Figure 3: A functional schematic of a 5-link, 2-DOF basic planetary gear train.

where ω_i is the angular speed of link i and gear ratios $\gamma_{41} = -Z_4/Z_1$ and $\gamma_{42} = +Z_4/Z_2$. The positive sign of the gear ratio represents an internal gear pair, and the negative sign depicts an external gear pair. The symbol Z_i is the number of teeth on gear i. By eliminating ω_4 from (1), the kinematic equation of a basic planetary gear train is

$$\omega_1 - \gamma_{24}\gamma_{41}\omega_2 + (\gamma_{24}\gamma_{41} - 1)\,\omega_3 = 0, \tag{2}$$

where the gear ratio $\gamma_{24} = 1/\gamma_{42}$. As mentioned in Section 2, the sun gear (Member 1) is designated as the fixed link, while the ring gear (Member 2) or the planet arm (Member 3) serves as the input link or the output link for the proposed speed-changing wheel hub. Therefore, three different arrangements are listed in Table 1. The speed ratio (SR) is defined as the ratio of the input link speed to the output link speed, while the SR formula can be derived from the kinematic equation shown in (2). It is found that the SR formulas of Case 1 and Case 2 are reciprocal. Since the SR of Case 1 is greater than one, that is, $(\gamma_{24}\gamma_{41} - 1)/\gamma_{24}\gamma_{41} > 1$, it is an underdrive. The SR of Case 2 is less than one; that is, $0 < \gamma_{24}\gamma_{41}/(\gamma_{24}\gamma_{41} - 1) < 1$; it is an overdrive. The SR of Case 3 is equal to one; it is a direct drive. Therefore, the proposed three-speed wheel hub provides an underdrive for the low-speed gear (Gear I), a direct drive (Gear II), and an overdrive for the high-speed gear (Gear III). We let the SR of Gear I be 4/3 for the low-speed driving; that is, $(\gamma_{24}\gamma_{41} - 1)/\gamma_{24}\gamma_{41} = 4/3$; then, we have $3Z_1 = Z_2$. Due to the limited installation space of the rear fork, the minimum number of teeth of sun gear Z_1 is selected as 18 to avoid gear interference, when the module is equal to 1. Because the number of teeth of planet gear Z_4 does not affect the SR, the minimum number of teeth of planet gear Z_4 is also selected as 18. A set of feasible solutions for the number of teeth on the sun gear, planet gear, and ring gear are $Z_1 = 18$, $Z_4 = 18$, and $Z_2 = 54$, respectively. For the direct drive, the input link can be designated as the ring gear (Member 2) or the planet arm (Member 3). Based on the engineering reality, the power transmission path from the rotor (Member 6) of the BLDC motor to the hub shell (Member 9) via the ring gear (Member 2) is shorter than that via the planet arm (Member 3). Due to this, the input link of Gear II is selected as the ring gear (Member 2). The related clutching sequence table and the SR of each gear of the proposed three-speed wheel hub are shown in Table 2, where the symbol "X" denotes that the corresponding clutch is engaged. It is noted that only one clutch is engaged while another is simultaneously disengaged during speed ratio changes, so, the proposed three-speed wheel hub is operated with a single clutch-to-clutch shaft. This is an important feature for a mechanical wheel hub to shift smoothly from one speed to another.

Table 1: Speed ratio at each speed of the three-speed wheel hub.

Case	Fixed link	Input link	Output link	SR formula
I	1	2	3	$(\gamma_{24}\gamma_{41} - 1)/\gamma_{24}\gamma_{41}$
II	1	3	2	$\gamma_{24}\gamma_{41}/(\gamma_{24}\gamma_{41} - 1)$
III	1	2 (3)	2 (3)	1

4. Design of an Exterior-Rotor BLDC Hub Motor

The design of a BLDC hub motor is an iterative process, where many unknown parameters are involved. One important task is to check whether the electromagnetic torque of the hub motor is sufficient to propel an electric bicycle. In general, the rated torque about of 15 Nm is required for an electric bicycle. A 350 W, 3-phase, 12-pole/18-slot BLDC hub motor with an exterior-rotor configuration has been designed as part of the integrated device for use in electric bicycles. Figure 4 illustrates the geometry of the designed BLDC hub motor that contains a cross-sectional view and related geometric parameters. Table 3 shows the rated conditions, magnet's material properties, and design results for the exterior-rotor BLDC hub motor. The permanent magnet is selected as the neodymium-iron-boron (NdFeB) BNP12. The winding configurations of each phase for the BLDC hub motor are schematically shown in Figure 5. A two-dimensional FEA package Ansoft/Maxwell has been employed in the magnetic field analysis and electromagnetic torque calculation of the hub motor. The flux density distribution within the air gap is shown in Figure 6. We can find that the dips in the air gap flux density occur at 15 and 42 mechanical degrees, which are caused by stator slot openings. The pulsation of the air gap flux density is pronounced under a fixed region near the dips, which may be induced by the flux concentrating effect. Figure 7 shows the three-phase flux linkage waveforms of this BLDC hub motor obtained from the software simulation. The period of the flux linkage waveform is equal to 360 electrical degrees, that is, 60 mechanical degrees for this hub motor with 6 magnet pole pairs. The waveforms of the three-phase back-EMF constant without multiplying the number of coils are presented in Figure 8. It can be found

Table 2: A clutching sequence table of the proposed three-speed wheel hub.

Gear	Clutch				
	C_{i2}	C_{o2}	C_{i3}	C_{o3}	SR
Low-speed gear (Gear I)	X			X	1.33
Direct drive (Gear II)	X	X			1.00
High-speed gear (Gear III)		X	X		0.75

Table 3: Rated conditions, magnet's material properties, and design results for an exterior-rotor BLDC hub motor.

Items	Symbol	Values
Rated conditions		
Rated power (W)	P_R	350
Rated speed (rpm)	ω_R	300
Magnet's material properties (NdFeB BNP12)		
Remanence (T)	B_r	0.76
Relative permeability	μ_r	1.26
Coercivity (A/m)	H_c	−480000
Direction of magnetization	—	Parallel
Magnet thickness (mm)	l_m	2
Magnet arc (degree)	θ_m	27
Design results		
Number of phases	N_{ph}	3
Number of magnet poles	P	12
Number of armature slots	S	18
Air-gap length (mm)	g	0.5
Slot opening (mm)	W_s	2.6
Inner radius of rotor (mm)	R_{ri}	50.5
Outer radius of rotor (mm)	R_{ro}	60
Inner radius of stator (mm)	R_{si}	20
Outer radius of stator (mm)	R_{so}	50
Tooth width of stator (mm)	w_{tb}	7
Shoe depth (mm)	d_1	2
Shoe ramp (degree)	d_2	0
Number of coils per armature tooth (turn)	N_c	54
Stack length (mm)	L	80
Rated phase current (A)	i_{ph}	8.3

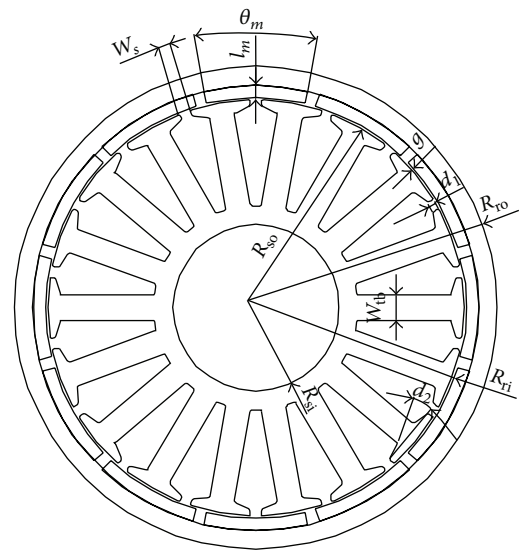

Figure 4: Cross-section and geometric parameters of the BLDC hub motor.

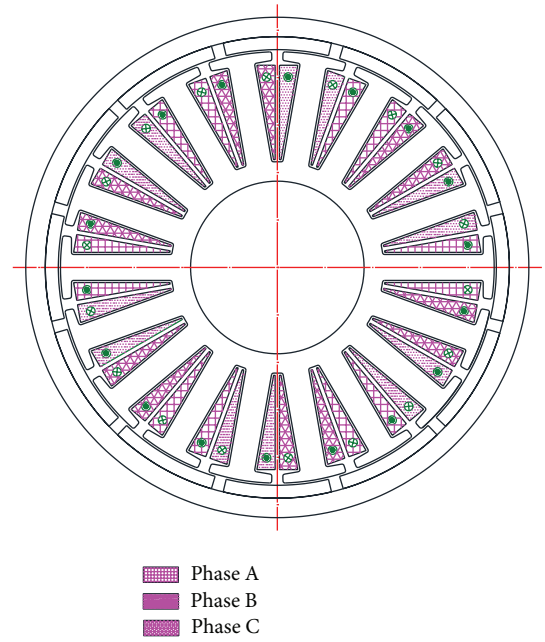

Figure 5: Winding configurations of each phase for the BLDC hub motor.

that a concave portion, which is caused by the stator slot opening on the stator, occurs on the flat top of the back-EMF constant waveform. The back-EMF constant waveform of each phase is similar to a trapezoidal wave shape, so each phase current of this motor is suitable to operate with square-wave excitation, as shown in Figure 9. The electromagnetic torque generated by this BLDC hub motor based on the FEA simulation is demonstrated in Figure 10. The average electromagnetic torque of this BLDC hub motor is 19.67 Nm, which is sufficient to propel an electric bicycle.

5. Analysis of Power Transmission Path

The validity for the operation of the integrated device at each gear can be checked by analyzing the related power transmission path. At a low-speed gear (Gear I), pawl-and-ratchet clutches C_{i2} and C_{o3} are simultaneously engaged according to the clutching sequence table, shown in Table 2. The shift control sleeve (Member 8) is in its left position. The pawl of clutch C_{o2} is controlled by the flange of the shift control sleeve (Member 8) to be unengaged, as sketched in Figure 11, while clutch C_{i3} is also controlled to be unengaged. The power from the rotor yoke (Member 6) of the BLDC hub motor is transmitted via clutch C_{i2} to the ring gear (Member 2), the planet gear (Member 4), the planet arm (Member 3), clutch C_{o3}, and finally, to the hub shell (Member 9), as shown

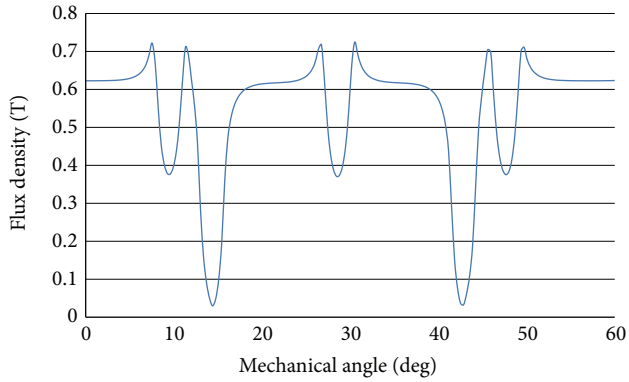

Figure 6: Air gap flux density of the BLDC hub motor.

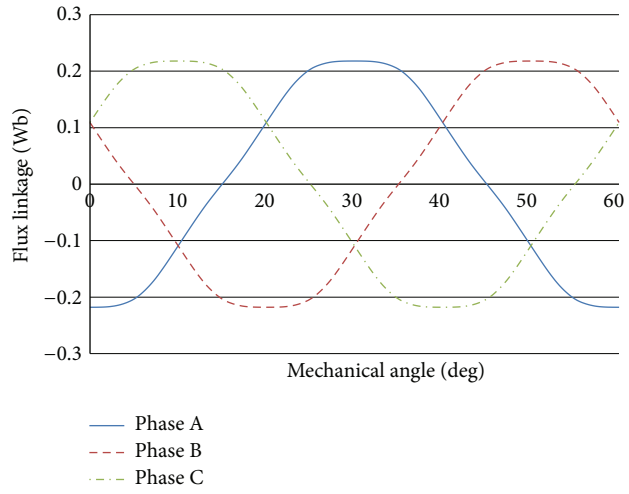

Figure 7: Three-phase flux linkage waveforms of the BLDC hub motor.

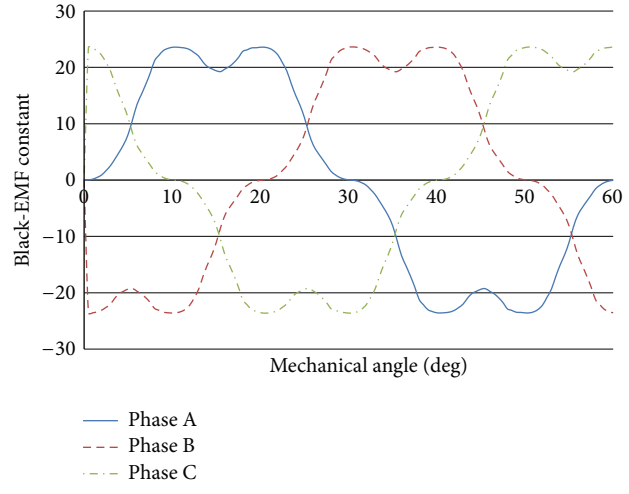

Figure 8: Three-phase back-EMF constant waveforms of the BLDC hub motor.

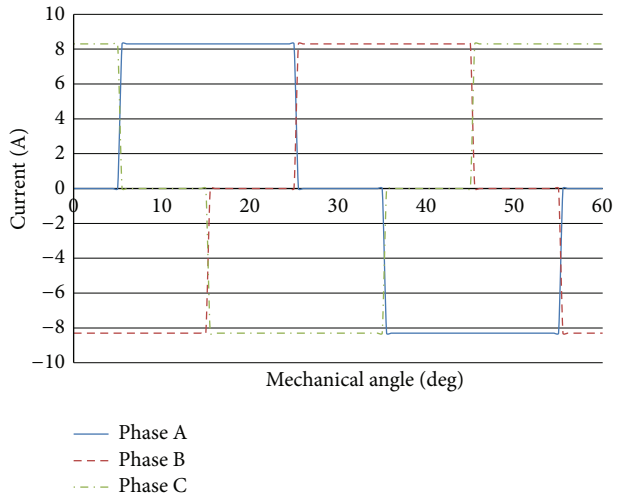

Figure 9: Three-phase excitation current waveforms of the BLDC hub motor.

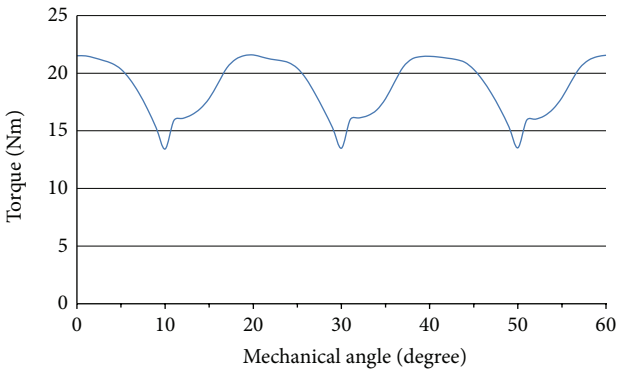

Figure 10: Electromagnetic torque generated by the BLDC hub motor.

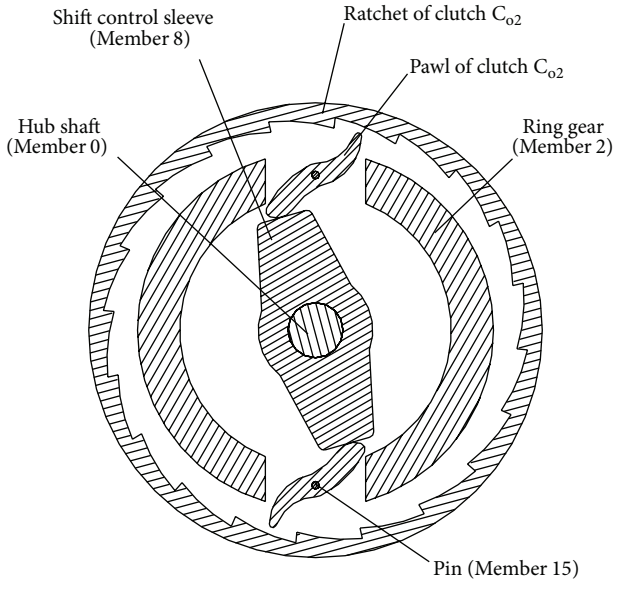

Figure 11: The pawl of clutch C_{o2} is controlled by the flange of the shift control sleeve to be unengaged.

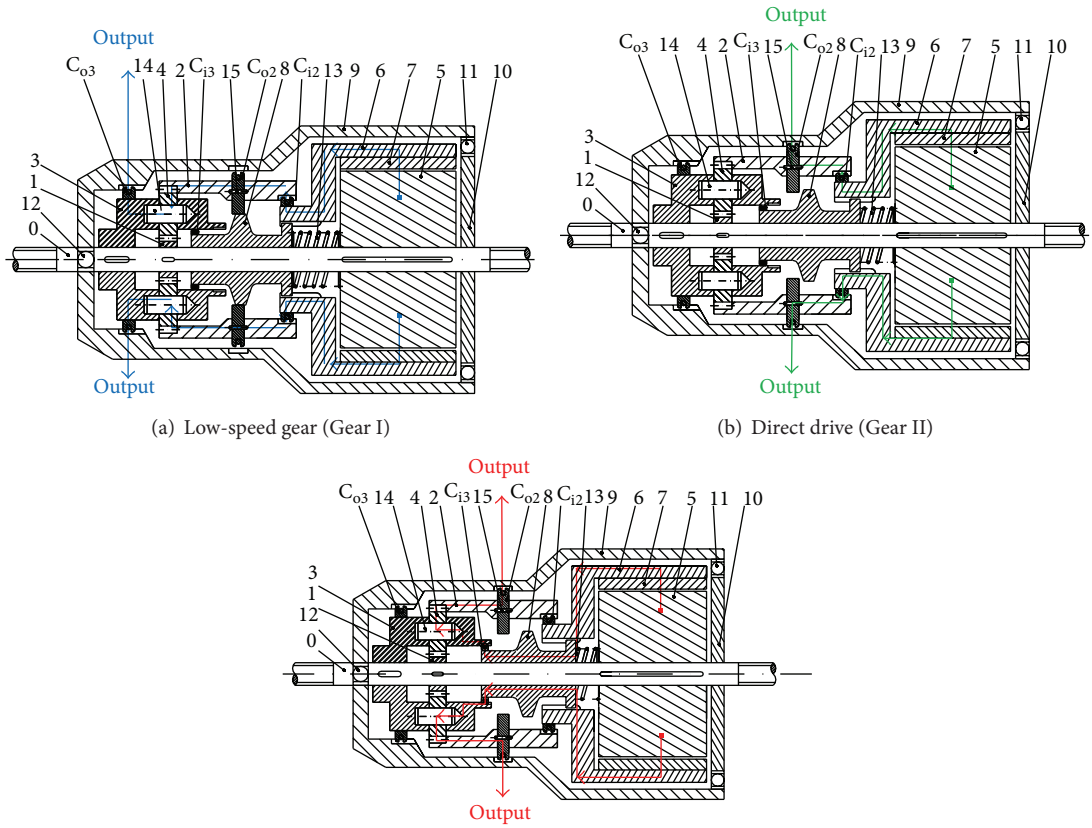

(a) Low-speed gear (Gear I)

(b) Direct drive (Gear II)

(c) High-speed gear (Gear III)

FIGURE 12: Power transmission path at each gear of the integrated device.

in Figure 12(a). At the direct drive (Gear II), the shift control sleeve (Member 8) is axially shifted to the middle position along the stationary hub shaft. Since the pawl of clutch C_{o2} is no longer controlled by the flange of the shift control sleeve (Member 8), it is engaged with the ratchet portion on the hub shell (Member 9) due to the action of a torsion spring stored at a pin (Member 15), as shown in Figure 13. At Gear II, only clutch C_{i3} is controlled to be unengaged. The power from the rotor (Member 6) of the BLDC hub motor at this speed is transmitted via clutch C_{i2}, the ring gear (Member 2), clutch C_{o2}, and then, directly to the hub shell (Member 9), as shown in Figure 12(b). When the shift control sleeve (Member 8) is further shifted to the right position, the integrated device is at a high-speed gear (Gear III). The pawl of clutch C_{i3} on the shift control sleeve (Member 8) is engaged with the ratchet on the planet arm (Member 3), thereby activating clutch C_{i3}. Since the rotational speed of the ring gear (Member 2) is faster than that of the planet arm (Member 3) at Gear III, clutch C_{o2} is engaged. As shown in Figure 12(c), the power from the rotor (Member 6) of the BLDC hub motor is transmitted via the shift control sleeve (Member 8), clutch C_{i3}, the planet arm (Member 3), the planet gear (Member 4), the ring gear (Member 2), clutch C_{o2}, and finally, to the hub shell (Member 9). Based on the above analyses, three forward speeds of the proposed design can be successfully achieved.

6. Conclusion

A novel electromechanical device integrating an electric motor within a speed-changing wheel hub is presented for electric bicycle applications. A 5-link, 2-DOF planetary gear mechanism is employed to provide three forward speeds, including an underdrive (SR = 1.33), a direct drive (SR = 1.00), and an overdrive (SR = 0.75). A speed-changing control mechanism is designed and installed within the planetary gear mechanism to manually control four pawl-and-ratchet clutches, which govern the power transmission path at each gear. A set of feasible solutions for the number of gear-teeth of the planetary gear mechanism is further synthesized based on the fundamental circuit equations. A 350 W, 3-phase, 12-pole/18-slot BLDC hub motor with an exterior-rotor configuration is designed as the power source of the integrated device by using commercial finite-element analysis package Ansoft/Maxwell. The average electromagnetic torque of this BLDC hub motor is 19.67 Nm, which is sufficient for electric bicycle applications. Such an integrated device overcomes inherent drawbacks of existing products. Although the proposed device integrates an exterior-rotor BLDC motor with a basic planetary gear train, it can be extended to the integration of other types of electric motors with a multispeed wheel hub for providing better output performance and more forward speed ratios.

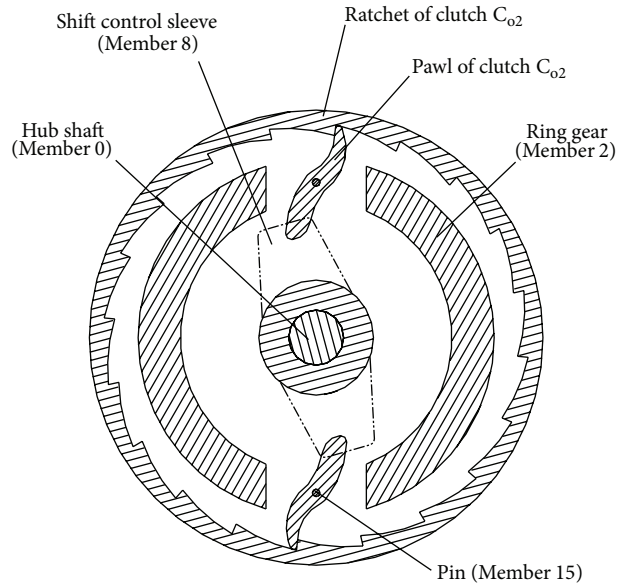

FIGURE 13: The pawl of clutch C_{o2} engaged with the ratchet portion on the hub shell.

Acknowledgment

The authors are grateful to the National Science Council (Taiwan) for supporting this research under Grant NSC 102-2221-E-224-016-MY2.

References

[1] *Giant Bicycles Catalog*, Giant Bicycle, Taipei, Taiwan, 2013.

[2] Y. C. Wu and P. W. Ren, "Design and analysis of a multispeed transmission hub," *INFORMATION*, vol. 16, no. 9(B), pp. 7003–7014, 2013.

[3] C.-H. Hsu and Y.-C. Wu, "Automatic detection of embedded structure in planetary gear trains," *Journal of Mechanical Design, Transactions of the ASME*, vol. 119, no. 2, pp. 315–318, 1997.

[4] Y. C. Wu and S. L. Lin, "Conceptual design of a 16-speed bicycle drive hub," *Applied Mechanics and Materials*, vol. 52–54, pp. 279–284, 2011.

[5] Z. Q. Zhu, D. Howe, and C. C. Chan, "Improved analytical model for predicting the magnetic field distribution in brushless permanent-magnet machines," *IEEE Transactions on Magnetics*, vol. 38, no. 1, pp. 229–238, 2002.

[6] B. Han, S. Zheng, and X. Liu, "Unbalanced magnetic pull effect on stiffness models of active magnetic bearing due to rotor eccentricity in brushless DC motor using finite element method," *Mathematical Problems in Engineering*, vol. 2013, Article ID 745912, 10 pages, 2013.

[7] C.-H. Hsu and R.-H. Huang, "Systematic design of six-speed automatic transmissions with an eight-link two-DOF Ravigneaux gear mechanism," *Journal of Mechanical Design, Transactions of the ASME*, vol. 131, no. 1, Article ID 0110041, 8 pages, 2009.

[8] W. H. Hsieh, "Kinetostatic and mechanical efficiency studies on cam-controlled planetary gear trains—part I theoretical analysis," *Indian Journal of Engineering and Materials Sciences*, vol. 20, no. 3, pp. 191–198, 2013.

[9] F. Freudenstein and A. T. Yang, "Kinematics and statics of a coupled epicyclic spur-gear train," *Mechanism and Machine Theory*, vol. 7, no. 2, pp. 263–275, 1972.

[10] L.-C. Hsieh and H.-S. Yan, "Generalized kinematic analysis of planetary gear trains," *International Journal of Vehicle Design*, vol. 13, no. 5-6, pp. 494–504, 1992.